J. Meas. Sci. Instrum., 2025, 16(3): 406-414. http://jmsi.publish.founderss.cn
DOI: 10.62756/jmsi.1674-8042.2025039 jmsi@nuc.edu.cn

A BDS/SINS integrated positioning approach for trains in complicated operation scenes

WU Xiaochun*, YANG Weikang

School of Automation & Electrical Engineering, Lanzhou Jiaotong University, Lanzhou 730070, China

***Corresponding author:** WU Xiaochun (369038806@qq.com)

Received: November 28, 2023 **Revised:** January 5, 2024 **Accepted:** January 14, 2024

Abstract: The traditional train positioning methods suffer from inadequate accuracy and high maintenance costs, rendering them unsuitable for the development requirements of lightweight and intelligent train positioning technology. To address these restraints, the BeiDou navigation satellite system/strapdown inertial navigation system (BDS/SINS) integrated train positioning system based on an adaptive unscented Kalman filter (AUKF) is proposed. Firstly, the combined denoising algorithm (CDA) and Lagrange interpolation algorithm are introduced to preprocess the original data, effectively eliminating the influence of noise signals and abnormal measurements on the train positioning system. Secondly, the innovation theory is incorporated into the unscented Kalman filter (UKF) to derive the AUKF, which accomplishes an adaptive update of the measurement noise covariance. Finally, the positioning performance of the proposed AUKF is contrasted with that of conventional algorithms in various operation scenes. Simulation results demonstrate that the average value of error calculated by AUKF is less than 1.5 m, and the success rate of positioning touches 95.0%. Compared to Kalman filter (KF) and UKF, AUKF exhibits superior accuracy and stability in train positioning. Consequently, the proposed AUKF is well-suited for providing precise positioning services in variable operating environments for trains.

Key words: train integrated positioning; BeiDou navigation satellite system (BDS); strapdown inertial navigation system (SINS); Lagrange interpolation algorithm; combined denoising algorithm (CDA); adaptive unscented Kalman filter (AUKF)

0 Introduction

With the increasing speed and density of trains on railways, there is a growing demand for an advanced train operation control system to effectively command train operation. As the essence of the train control system, high-precision train positioning can shorten the train tracking interval and improve the transportation efficiency of the railway industry. Currently, track circuits, balises, and odometers are commonly employed on high-speed railway lines to measure train velocity and position. The traditional positioning methods necessitate the installation of extensive trackside equipment, resulting in substantial operational and maintenance costs. Consequently, it fails to meet the positioning technical requirements of the new train control system.

The BeiDou navigation satellite system (BDS) has developed rapidly in recent years and widely applied to vehicle positioning and driving assistance[1]. Furthermore, during the initial phase of the Qinghai-Tibet railway operation, the enhanced train control system based on global position system is employed to facilitate train dispatch commands, which provides reference and support for the implementation of BDS in train positioning. The railway operation scenes are very elaborate, characterized by constantly changing satellite occlusion. Hence, relying solely on BDS cannot satisfy the availability, continuity, and reliability of train positioning. To address this limitation, an integrated positioning technology combines BDS with other positioning methods to form multi-source positioning information, which mitigates the drawbacks of individual system. Since strapdown inertial navigation system (SINS) remains impervious to external factors and consistently provides comprehensive positioning information, the integration of BDS and SINS in train positioning establishes a complementary relationship, which meets the technical requirements of this domain[2].

The fusion of positioning information is crucial in the train's integrated positioning system as it directly impacts the accuracy of train positioning[3]. The unscented Kalman filter (UKF) is widely employed for target tracking and motion carriers positioning[4]. However, the parameters of

UKF, such as system noise covariance and measurement noise covariance, remain constant, failing to account for the influence of satellite occlusion along the railway on the integrated positioning system. Mismatching of noise estimation characteristics may lead to the increase of train positioning error or even filter divergence[5]. Therefore, numerous scholars made improvements to the UKF. Li et al.[6] introduced an adaptive fading factor into UKF, which effectively corrects outliers in the filter and reduces the influence of previous data on the current data. The positioning results demonstrate that the improved UKF achieves positioning errors of less than 4 m under good satellite signal conditions. Bahraini et al.[7] added an adaptive scale factor in the process of UKF and used the adaptive random search maximization approach to select the optimal adaptive scale factor, thereby improving the accuracy of filter estimation. Gu et al.[8] proposed an improved UKF based on the adaptive fading factor, which curtails the influence of past observations on the filtering accuracy, consequently enhancing the positioning accuracy and reliability of the integrated positioning system.

After analyzing the literature works of domestic and foreign scholars, the following conclusions emerge:

1) Many scholars directly deliver the raw data from the inertial measurement unit (IMU) and satellite measurements collected by the onboard sensor to the train integrated positioning system for positioning calculation. Nevertheless, the train operating environment is complex, and mechanical vibration, electromagnetic environment interference, and satellite occlusion environment may affect the quality of the collected data. Consequently, intelligent algorithms are necessary to preprocess the original data collected by the positioning sensor prior to obtaining an accurate positioning solution.

2) Introducing an adaptive factor into the UKF can enhance positioning performance, However, constructing the adaptive factor entails increasing the types of measurement values or reliable measurement information. On one hand, increasing the number of measurement values will complicate the algorithm and reduce real-time calculation performance. On the other hand, the complex operating environment along the railway may introduce interference with received satellite signals, resulting in gross errors of the measurement data.

Consequently, this study employs a combined denoising method to enhance the quality of the IMU original data. Additionally, the Lagrange interpolation algorithm is utilized to smoothen the satellite measurements, ensuring the accuracy of the original data. Subsequently, while maintaining the original observation value, the UKF is improved based on the innovation theory. The obtained adaptive unscented Kalman filter (AUKF) achieves the adaptive update of the measurement noise covariance, thereby improving the accuracy of filtering estimation and diminishing the error in train positioning. Lastly, the suitability and effectiveness of the proposed AUKF algorithm for the train integrated positioning system are illustrated through simulation comparison experiments.

1 Integrated train positioning system

The train integrated positioning system enables the long-term and continuous positioning services for trains operating in unpredictable operating environments. By integrating multiple systems, it delivers more accurate and reliable information compared to individual systems. Fig. 1 illustrates the overall structure of the train integrated positioning system, utilizing the BeiDou satellite receiver and IMU as onboard positioning sensors. The train achieves its positioning function through a series of processes, including information collection, data preprocessing, positioning information fusion, and the output of positioning results.

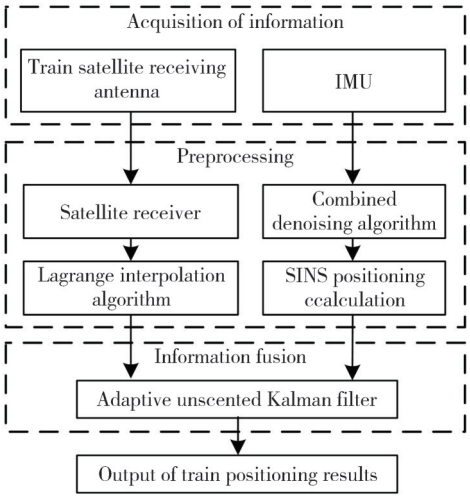

Fig. 1 Framework of train integrated positioning system

2 Preprocessing of positioning data

2.1 IMU raw data denoising

The electromagnetic environment in railway operations exhibits significant variability, which poses interference challenges in collecting and transmitting sensor-based positioning information. The mechanical vibration generated by the train movement introduces noise signals into IMU, such as accelerometer and gyroscope. These noise signals seriously affect the usability of IMU raw data, resulting in a decline in train positioning accuracy. Therefore, denoising of the

collected IMU raw data is essential prior to the calculation and fusion of train positioning information.

The complementary ensemble empirical mode decomposition (CEEMD) is a suitable approach for nonlinear and non-stationary signal processing. However, during the signal reconstruction phase of CEEMD denoising, the intrinsic mode function (IMF) that contains noise signals is directly discarded, leading to the loss of valuable information and potential distortion of the original signal[9]. To overcome this shortcoming, a combined denoising algorithm (CDA) is proposed, harnessing the strengths of both CEEMD and wavelet threshold denoising. The wavelet threshold denoising processes the high-frequency IMF obtained by CEEMD decomposition. Then the denoised IMF and other IMFs are superimposed to reconstruct the signal. The CDA can effectively erase the noise and retain the beneficial information of the IMU original signal. The process of CDA is depicted in Fig.2.

1) The original IMU signal is decomposed by CEEMD, and a series of IMFs spanning from high frequency to low frequency are obtained as

$$F_i(t)=\frac{1}{2n}\sum_{i=1}^{n}(F_{1,i}(t)+F_{2,i}(t)), \tag{1}$$

where $F_i(t)$ represents the ith IMF component, $F_{1,i}(t)$ is obtained by EMD of the signal with positive noise, $F_{2,i}(t)$ is obtained by EMD after adding negative noise, and multiple simulation comparisons show that the optimal decomposition layer i is 5.

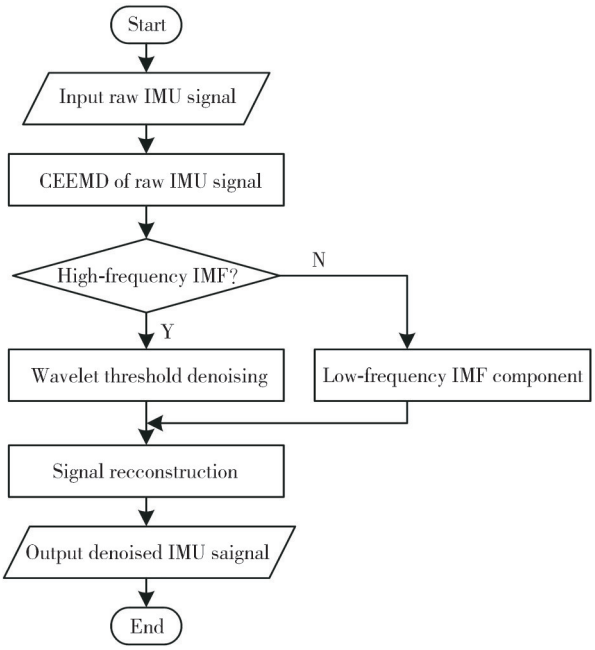

Fig. 2 Flow chart of combined denoising algorithm

2) The selection of the threshold function and threshold is crucial in wavelet threshold denoising. Conventional hard and soft threshold functions used for signal denoising may lead to a low signal-to-noise ratio in the reconstructed signal. To address this issue, this work introduces an improved wavelet threshold function as

$$\mu'(j,l)=\begin{cases}\operatorname{sgn}(\mu(j,l))\left(|\mu(j,l)|-\mathrm{e}^{\lambda(\beta-|\mu(j,l)|)}\beta\right), & |\mu(j,l)|\geqslant\beta,\\ 0, & |\mu(j,l)|<\beta,\end{cases} \tag{2}$$

where $\mu(j,l)$ is the wavelet coefficient, $\mu'(j,l)$ is the wavelet coefficient after filtering, β is the threshold, and λ is the adjustment factor with the value range of [0, 1].

Additionally, we adopt VisuShrink threshold, known for its strong adaptability, as the criterion for threshold determination, as shown in Fig.3. Its calculation process is

$$\beta=\sigma\sqrt{2\ln M}, \tag{3}$$

where M is the length of the signal, and σ is the root-mean-square deviation of noise.

3) The improved wavelet threshold denoising algorithm is used to denoise the high-frequency IMF obtained by CEEMD. Then, the signal is reconstructed to obtain the denoised IMFs.

4) The denoised IMFs and other IMFs are reconstructed to obtain the denoised IMU signal as

$$g(t)=\sum_{j=1}^{s}F_{\mathrm{h},j}(t)+\sum_{k=1}^{i-s}F_{\mathrm{d},k}(t), \tag{4}$$

where $F_{\mathrm{h},j}(t)$ is the jth high-frequency IMF after denoising, and $F_{\mathrm{d},k}(t)$ is the kth low-frequency IMF.

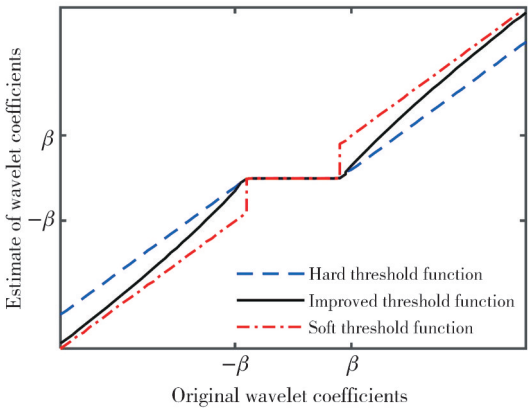

Fig. 3 Coordinate expression of threshold function

2.2 Smoothing of satellite measurements

In the presence of satellite occlusion during the train operation, environmental interference may lead to abnormal measurements in the received satellite signal. Incorporating aberrant measurements into positioning calculations can adversely impact the accuracy of results.

To mitigate this issue, the Lagrange interpolation algorithm is employed to smooth the original satellite measurements by eliminating the anomalous values. The Lagrange interpolation algorithm achieves global approximation of the measurements through the construction of interpolation polynomials. Let $y=f(x)$ represent a polynomial function, with the $k+1$ points of the polynomial denoted as (x_0,y_0), (x_1,y_1), $\cdots$, (x_k,y_k). The Lagrange interpolation polynomial is mathematically represented as

$$L(x)=\sum_{j=0}^{k} y_j l_j(x), \tag{5}$$

where $L(x)$ is the Lagrange interpolation polynomial, $l_j(x)$ is the basic function of interpolation, and its expression is

$$l_j(x)=\prod_{i=0,i\neq j}^{k}\frac{x-x_i}{x_j-x_i}. \tag{6}$$

During the train operation, if the abnormal measurements result in a large positioning error of the train at the time of $k+1$. The Lagrange interpolation algorithm is adopted to approximate the equivalent measurement. The calculation is depicted as

$$\begin{cases} l_0(t)=\dfrac{[t-t(k-1)][t-t(k)]}{[t(k-2)-t(k-1)][t(k-2)-t(k)]},\\ l_1(t)=\dfrac{[t-t(k-2)][t-t(k)]}{[t(k-1)-t(k-2)][t(k-1)-t(k)]},\\ l_3(t)=\dfrac{[t-t(k-1)][t-t(k-2)]}{[t(k)-t(k-1)][t(k)-t(k-2)]},\\ z(k+1)=\hat{z}(k-2)l_0(t)+\hat{z}(k-1)l_1(t)+\hat{z}(k)l_2(t), \end{cases} \tag{7}$$

where $l_0(t)$, $l_1(t)$ and $l_2(t)$ are the basic functions of interpolation, and $t(k)$ is the step.

3 Fusion of positioning information

3.1 Standard UKF

The train integrated positioning system is a robust nonlinear system. Its discrete-time state equation and measurement equation are expressed as

$$\begin{cases} \boldsymbol{X}_k=f(\boldsymbol{X}_{k-1})+\boldsymbol{W}_{k-1},\\ \boldsymbol{Z}_k=\boldsymbol{H}_k\boldsymbol{X}_k+\boldsymbol{V}_k, \end{cases} \tag{8}$$

where $\boldsymbol{X}_k$ is the 15-dimensional state vector of the train integrated positioning system, $f(\boldsymbol{X}_{k-1})$ is the nonlinear function of the system, $\boldsymbol{W}_{k-1}$ is the process noise; $\boldsymbol{V}_k$ is the measurement noise, and $\boldsymbol{H}_k$ is the measurement transfer matrix of the system.

UKF is a commonly utilized algorithm for handling nonlinear systems. It employs an optimal sampling strategy to obtain sigma points. The acquired sigma sample points are mapped according to the nonlinear system function[12]. The statistical properties of these mapped sigma sample points are calculated to represent the probability distribution of the state variables of the nonlinear system. The UKF process can be summarized as the following algorithm shown in Table 1.

Table 1 Pseudocode of UKF

Algorithm: UKF
Input: $\boldsymbol{Q}_k,\boldsymbol{R}_k,\hat{\boldsymbol{X}}_0,\hat{\boldsymbol{P}}_0$
For $k=1:N$
  Initialization: $\boldsymbol{X}_0=\hat{\boldsymbol{X}}_0$, $\boldsymbol{P}_0=\hat{\boldsymbol{P}}_0$
  Time update stage (at $k-1$ moment):
    Sigma sample points χ^i_{k-1};
    Weights $\omega^b_0,\omega^c_0,\omega^b_i,\omega^c_i$;
    Calculate prior state estimates $\hat{\boldsymbol{X}}_{k/k-1}$;
    Compute error covariance matrix $\hat{\boldsymbol{P}}_{k/k-1}$;
  Measurement update stage (at k moment):
    Predicted sigma sample points $\chi^i_{k/k-1}$;
    Calculate the mean of predicted measurements $\boldsymbol{Z}_{k/k-1}$;
    Compute covariance $\boldsymbol{P}_{k/k-1}$;
    Calculate cross-covariance $\boldsymbol{P}_{Z,k/k-1}$;
    Obtain Kalman gain $\boldsymbol{K}_k$;
    Update state estimation $\hat{\boldsymbol{X}}_k$ and covariance $\boldsymbol{P}_k$.
End for
Output: posterior state estimation $\hat{\boldsymbol{X}}_k$ and error covariance matrix $\boldsymbol{P}_k$

3.2 Adaptive UKF

The use of fixed parameters, such as system noise covariance and measurement noise covariance, in the UKF does not account for environmental changes during the train operation, leading to a decrease in the positioning performance of the train integrated positioning system. To address this limitation, the calculation of innovation is introduced to the UKF. The innovation represents the disparity between the actual measurement and the predicted value of the sensor, innovation is calculated by

$$\boldsymbol{Q}_k=\boldsymbol{Z}_k-\hat{\boldsymbol{Z}}_k, \tag{9}$$

where $\boldsymbol{Q}_k$ is the innovation value, $\boldsymbol{Z}_k$ is the actual measured value, and $\hat{\boldsymbol{Z}}_k$ is the calculated posterior measurement.

By incorporating the innovation into the UKF, the positioning performance can be improved. The specific process for incorporating the innovation is outlined as follows:

1) The judgment of adaptive condition. The posterior state estimation value of the train integrated positioning system is $\boldsymbol{X}_k$. The discrepancy between the posterior state estimation value and the theoretical optimal value can be quantified by

$$\boldsymbol{D}_k=\boldsymbol{Q}_k^{\mathrm{T}}\boldsymbol{R}_k^{-1}\boldsymbol{Q}_k, \tag{10}$$

where $\boldsymbol{D}_k$ is the posterior Mahalanobis distance. If the distance exceeds a predefined threshold, it indicates a

failure to meet the positioning requirements. In such a case, an update of the measurement noise covariance is necessary based on the innovation. The threshold is set to the chi-square value, as specified in Table 2. Distinct thresholds are established for measurement vectors of varying dimensions.

Table 2 Partial chi-square distribution

Degree of confidence	χ^2 (6d)	χ^2 (7d)	χ^2 (8d)	χ^2 (9d)
0.995	0.68	0.99	1.34	1.73
0.990	0.87	1.24	1.65	2.09
0.950	1.64	2.17	2.73	3.33
0.900	2.20	2.83	3.40	4.17
0.750	3.45	4.25	5.07	5.90
0.500	5.35	6.35	7.34	8.34
0.250	7.84	9.04	10.22	11.39
0.100	10.64	12.02	13.36	14.68
0.050	12.59	14.07	15.51	16.92

* 6d, 7d, 8d and 9d represent six-, seven-, eight- and nine-dimensional, respectively.

2) Update of measurement noise covariance $\boldsymbol{R}_k$. According to the measurement equation of the system and the definition of innovation, innovation value is rewritten as

$$\boldsymbol{Q}_k = \boldsymbol{H}_k(\boldsymbol{X}_k - \hat{\boldsymbol{X}}_{k/k-1}) + \boldsymbol{V}_k. \tag{11}$$

The difference between the actual and the prior state estimation value is defined as $\Delta\boldsymbol{X}_{k/k-1}$. The covariance of innovation is calculated by

$$E(\boldsymbol{Q}_k\boldsymbol{Q}_k^{\mathrm{T}}) = \boldsymbol{H}_k E[\Delta\hat{\boldsymbol{X}}_{k/k-1}\Delta\hat{\boldsymbol{X}}_{k/k-1}^{\mathrm{T}}]\boldsymbol{H}_k^{\mathrm{T}} + \boldsymbol{R}_k. \tag{12}$$

The expected value of the innovation covariance can be estimated by

$$E(\boldsymbol{Q}_k\boldsymbol{Q}_k^{\mathrm{T}}) = \frac{1}{k}\sum_{i=1}^{k}(\boldsymbol{Q}_k^i - \bar{\boldsymbol{Q}}_k)(\boldsymbol{Q}_k^i - \bar{\boldsymbol{Q}}_k)^{\mathrm{T}}, \tag{13}$$

where $\bar{\boldsymbol{Q}}_k$ is the average value of all innovations.

By combining Eqs. (12) and (13), measurement noise covariance can be expressed as

$$\boldsymbol{R}_k = E(\boldsymbol{Q}_k\boldsymbol{Q}_k^{\mathrm{T}}) - \boldsymbol{H}_k E(\Delta\boldsymbol{X}_{k/k-1}\Delta\boldsymbol{X}_{k/k-1}^{\mathrm{T}})\boldsymbol{H}_k^{\mathrm{T}}. \tag{14}$$

4 Experiments and analysis

4.1 Construction of simulation environment

A simulation platform for the train integrated positioning system was established based on the guidelines provided by the precise strapdown inertial navigation system website and Ref.[11]. The positioning performance of the proposed train integrated positioning system was simulated and analyzed. The simulation parameters of the satellite receiver and IMU sensors on the train were set based on ATK1218 satellite positioning board and STIM300. The initialization of simulation parameters for the train integrated positioning system is presented in Table 3.

A specific section of the Sichuan-Tibet railway, stretching from Sangri station to Shannan station, is selected for analysis. The parameters of the simulation track are installed based on the satellite occlusion and length of the track.

Table 3 Initialization setting of simulation parameters

Parameter	Value
Initial velocity(v_E, v_N, v_U)/(m·s^{-1})	150, 150, 0
Roll, yaw and pitch angle/(°)	0, 0, 0
Bias of accelerometer/mg	0.05
Bias of gyro/((°)·h^{-1})	0.5
Resolution of accelerometer/mg	0.33
Resolution of gyro/((°)·h$^{-\frac{1}{2}}$)	0.007
Random walk error of accelerometer/(mg·h$^{-\frac{1}{2}}$)	0.06
Random walk error of gyro/((°)·h$^{-\frac{1}{2}}$)	0.15
Sampling frequency of IMU/Hz	100
Sampling frequency of BDS/Hz	10

Fig. 4 provides a visual representation of the actual train operating environment along the track, where the satellite visibility reflects the variations in different operating conditions. The evaluation of satellite visibility for the track is based on the total number of visible BeiDou satellites.

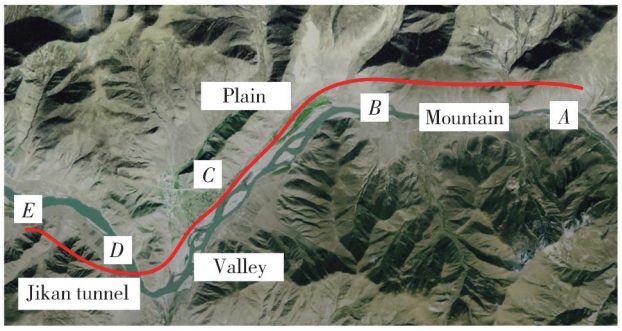

Fig. 4 Railway line from Sangri station to Shannan station

The train initiates its journey at coordinates 29.255°N, 92.159°E, and travels a total distance of 27.8 km at speeds ranging from 160 km·h^{-1} to 200 km·h^{-1}. In the *AB* section, covering a distance of 8.7 km through mountainous terrain, the onboard satellite receiver frequently encounters signal obstructions and reflections. The average number of visible satellites in this section is 4.1, indicating poor satellite visibility. The train passes through the open plain in the *BC* section, and the track length is 8.9 km. The average number of satellites is 13.4, and the satellite visibility is good. In the *CD* section, the train passes through a valley, resulting in certain satellites being inaccessible to the onboard receiver due to environmental occlusion. The average number of visible satellites in this section is 8.2, signifying ordinary satellite visibility. The *DE* section includes the Jikang tunnel, which is 1.296 km in length and where the satellite receiver fails to obtain any BeiDou satellite signal, resulting in zero visible satellites. Fig.5 provides a visual depiction of

the number of visible satellites along the track.

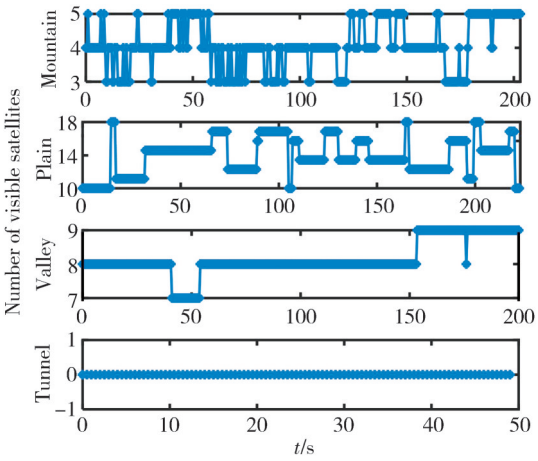

Fig. 5 Number of visible satellites along railway line

In order to quantitatively interpret the simulation results, root mean square error (RMSE) and average value of error (AVE) are selected as indicators. The calculation formulas are

$$RMSE=\sqrt{\frac{1}{n}\sum_{k=1}^{n}[x_p(k)-x_f(k)]^2}, \tag{15}$$

$$AVE=\frac{1}{n}\sum_{k=1}^{n}\left|x_p(k)-x_f(k)\right|, \tag{16}$$

where n is the number of samples, $x_p(k)$ is the state estimation value, and $x_f(k)$ is the true value.

4.2 Analysis of data preprocessing results

Firstly, the onboard IMU captures the initial angular rate and acceleration rate, which are subsequently processed using the CDA to obtain refined IMU data. Fig.6 presents a comparison between the denoised east angular rate and the original data. Subsequently, the measurements of the BeiDou satellite are handled by the Lagrange interpolation algorithm to obtain the smoothed data. Fig.7 demonstrates the data smoothing effect using longitude data collected during train operation as an illustrative example.

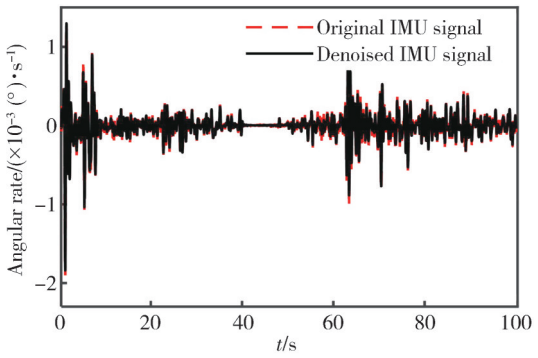

Fig. 6 Denoising comparison of IMU data

In Fig. 6, it is evident that the original IMU signal contains numerous noise artifacts, which are generated during the train operation. In contrast, the denoised IMU signal appears considerably smoother. Moreover, the overall trends of the two curves remain consistent. Hence, the CDA method effectively eliminates noise while preserving valuable information within the IMU signal, ensuring the accuracy of the original data for subsequent train positioning processes. Turning to Fig.7, the original longitude curve exhibits minor spikes, representing erroneous measurements obtained during the train operation. In contrast, the curve generated by the Lagrange interpolation algorithm appears more level. This observation illustrates the ability of the Lagrange interpolation algorithm to identify abnormal values and compute interpolated measurements that meet the positioning requirements.

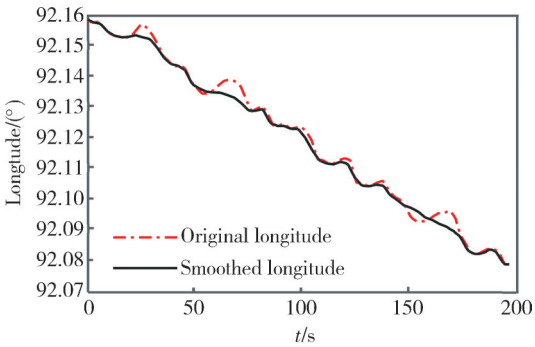

Fig. 7 Smooth comparison of longitudes

Different datasets are input into the train integrated positioning system for simulation analysis to verify the necessity of data preprocessing. The input datasets include:

1) Original IMU data and original measurements.
2) Denoised IMU data and original measurements.
3) Original IMU data and smoothed measurements.
4) Denoised IMU data and smoothed measurements.

The above datasets are input for positioning calculation, and the positioning results are quantitatively analyzed in Table 4.

Table 4 Positioning results on different datasets

Dataset	East		North	
	RMSE/m	AVE/m	RMSE/m	AVE/m
1	1.673	1.025	1.594	1.008
2	1.369	0.845	1.290	0.827
3	1.043	0.762	1.157	0.745
4	0.921	0.674	0.895	0.658

Table 4 provides a comprehensive analysis of the different datasets. The AVE calculated by the first dataset exceeds 1 m, and the RMSE outstrips 1.5 m, indicating the highest error among all datasets. It clarifies that the positioning results obtained from the original data are generally. Compared with the first dataset, the AVE calculated by the second dataset is decreased by

about 0.18 m, and the RMSE is diminished by about 0.3 m. This reduction highlights the effectiveness of CDA in purifying the IMU raw data and improving the accuracy of train positioning. Moreover, the third dataset demonstrates a decrease of 0.26 m in the AVE compared to the first dataset. It emphasizes the capability of the Lagrange interpolation algorithm in eliminating abnormal measurements and enhancing train positioning accuracy. Notably, the fourth dataset yields the smallest AVE and RMSE values, resulting in the highest positioning accuracy among all the datasets. Consequently, while using CDA or the Lagrange interpolation algorithm alone can optimize the positioning to a certain extent, the best positioning effect is achieved by jointly preprocessing the original IMU data and measurements.

4.3 Performance verification of AUKF

To assess the performance of the AUKF in various scenarios, simulations are conducted and validated. These scenarios include mountainous region, plain, valley, and tunnel. Comparative analysis is performed by considering the KF and UKF. The simulation conditions of KF and UKF are the same as AUKF. For example, the structure of BDS and SINS is loose coupling, and the input data are the denoised IMU data and the smoothed measurement.

Fig.8 presents the train positioning results obtained using different information fusion algorithms in diverse railway operation scenes.

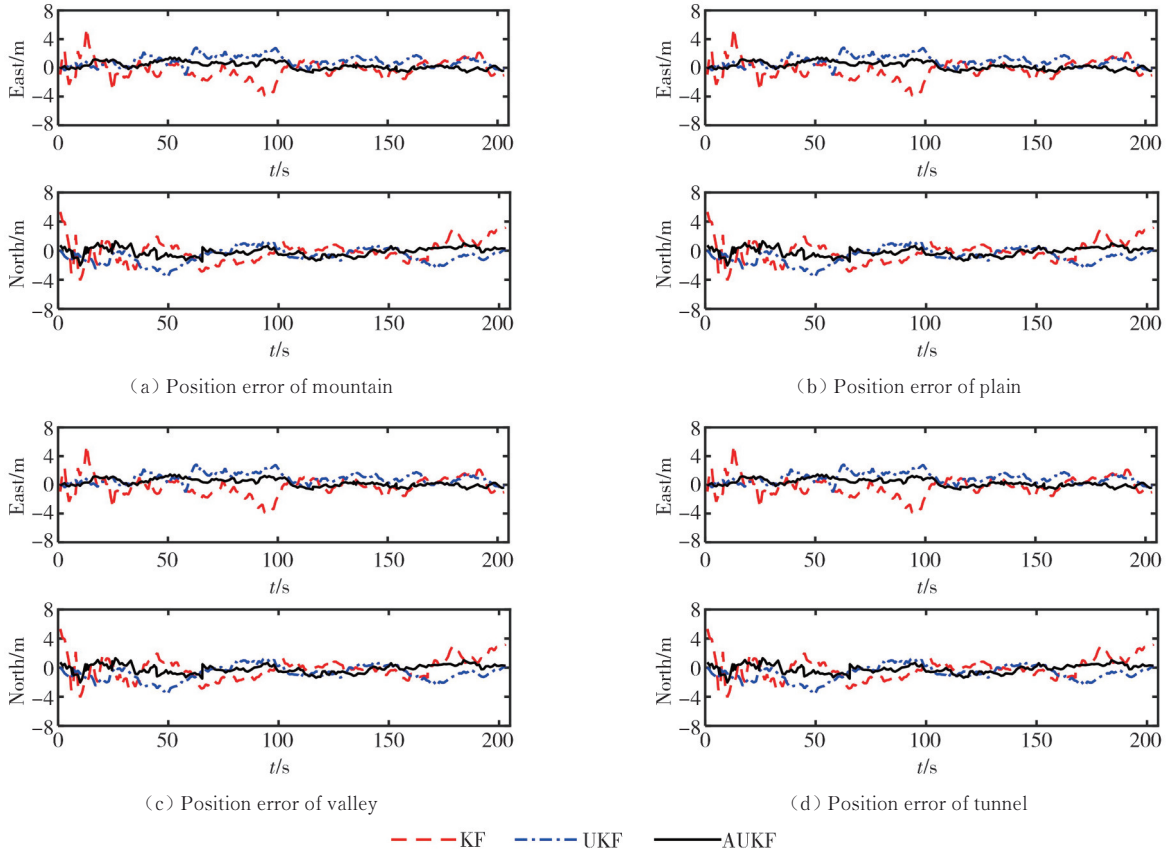

Fig. 8 Positioning errors in different scenes

The AVE obtained by quantitative analysis of the positioning results is displayed in Fig.9.

From the position error curve and AVE of the train, it can be inferred that KF exhibits a higher AVE within the same scene, accompanied by larger fluctuations in the error curve. Particularly when the train operates in a tunnel, the position error diverges significantly. The maximum error reaches 15 m, rendering the positioning result unacceptable. Although UKF shows an improvement in positioning error compared to KF, it still exceeds 5 m in scenes with poor satellite visibility, such as mountain and tunnel, failing to meet the technical requirements for railway train positioning. Conversely, The AVE obtained by AUKF is within 1.5 m. Compared with KF and UKF, AUKF has a positive positioning performance. In the same operating scene, the positioning error obtained by AUKF is more minor, and the error curve is steadier, making it an ideal choice for accurate train positioning.

The distance between centers of tracks is generally at

least 5 m. In order to correctly identify the section of train operation, the train positioning accuracy must reach 2.5 m[12]. Hence, this work defines the success rate of positioning as the proportion of epochs with a positioning error below 2.5 m. Fig. 10 presents the cumulative probability distribution of positioning errors throughout the train's positioning process.

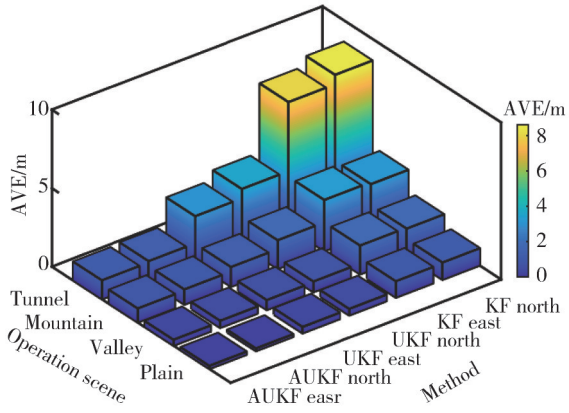

Fig. 9 AVE in different scenes

Fig. 10 clarifies that the success rate of positioning calculated by KF is only 42.6%, leading to positioning failures. Because KF is mainly used to deal with linear problems, while the train integrated positioning system represents a robust nonlinear system, making KF less adaptable. Comparatively, the success rate of positioning of UKF reaches 75.6%, which still cannot meet the continuity of train positioning. The success rate of positioning of AUKF exceeds 95.0%, providing credible results that guarantee the safe and reliable operation of trains on railway lines.

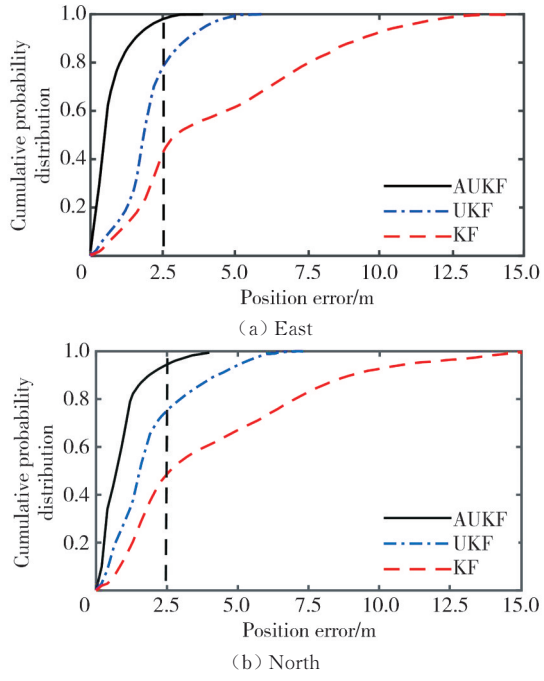

Fig. 10 Cumulative probability distribution of position error

In summary, in different operating environment, such as mountain, plain, valley, and tunnel, the positioning performance of AUKF is superior to that of KF and UKF. It displays enhanced resistance to interference and achieves higher success rates of positioning even in satellite occlusion scenes. Hence, the proposed AUKF algorithm proves to be well-suited for railway train positioning in complex operating environments

5 Conclusions

The main conclusions of research are as follows:

1) The train integrated positioning system utilizes the BeiDou satellite receiver and IMU as onboard sensors, effectively reducing the reliance on trackside equipment and lowering the operation and maintenance costs of the railway line. Moreover, it achieves accurate and continuous train positioning, making it highly valuable for engineering applications.

2) Through the data preprocessing process, such as denoising the original IMU data and smoothing the measured values, the error of the train positioning is decreased by 0.35 m, leading to improved accuracy in train positioning from the perspective of input data.

3) In various railway operation scenes, including plain, valley, mountain, and tunnel, the average positioning error of the train calculated using AUKF is less than 1.5 m, with a maximum error below 5 m. This approach effectively mitigates the problem of filtering divergence caused by mismatched noise estimation characteristics. The AUKF exhibits greater robustness and enhances the positioning stability of the train integrated positioning system compared to standard KF and UKF.

Acknowledgement

This work was supported by Project Fund of China National Railway Group Co., Ltd. (No.N2022G012), and Natonal Natural Science Foundation of China (No.61661027)

Declaration of conflicting interests

The authors have no conflict of interests related to this publication.

References

[1] TAO W J, CAI B G, LIU J, et al. Three-dimensional route generation method of digital track map based on UKF. Journal of Transportation Engineering, 2020, 20(5): 227-236.

[2] LIU J, TAN S L, CAI B G, et al. Cooperative weighting method for satellite-based vehicle positioning based on vehicle infrastructure information interaction. Transportation System Engineering and Information, 2022, 22(5): 85-96.
[3] SHANG G W, XIE Z X, JIANG W, et al. Optimization method of train integrated positioning based on IMU calibration compensation. Journal of the China Railway Society, 2020, 42(2): 57-64.
[4] SUN J R, TAO L, NIU Z, et al. An improved adaptive unscented Kalman filter with application in the deeply integrated BDS/INS navigation system. IEEE Access, 2020, 8: 95321-95332.
[5] LI P, YAN G H, CHEN G W, et al. Application of improved federated EKF in train integrated positioning. Journal of the China Railway Society, 2022, 44(9): 65-70.
[6] LI C H, MA J, YANG Y J, et al. Low-complexity adaptive cubature Kalman filter algorithm. Journal of Beijing University of Aeronautics and Astronautics, 2022, 48(4): 716-724.
[7] SUN R, ZHANG Z X, CHENG Q, et al. Pseudorange error prediction for adaptive tightly coupled GNSS/IMU navigation in urban areas. GPS Solutions, 2021, 26(1): 28.
[8] LI W D, YU Y, WANG Y M, et al. Train positioning information fusion algorithm based on sequential assisted adaptive fading UKF. Journal of Railway Science and Engineering, 2022, 19(7): 1838-1844.
[9] BAHRAINI M S. On the efficiency of SLAM using adaptive unscented Kalman filter. Iranian Journal of Science and Technology, Transactions of Mechanical Engineering, 2020, 44(3): 727-735.
[10] GU P, JING Z L, WU L B. Adaptive fading factor unscented Kalman filter with application to target tracking. Aerospace Systems, 2021, 4(1): 1-6.
[11] ZHOU K L, GUO C Y. Research on heart sound signal denoising by combining CEEMD and AFSA to optimize wavelet threshold. Manufacturing Automation, 2023, 45(1): 207-211.
[12] ZHOU W D, HOU J X. A new adaptive high-order unscented Kalman filter for improving the accuracy and robustness of target tracking. IEEE Access, 2019, 7: 118484-118497.
[13] SHEN C, XIONG Y F, ZHAO D H, et al. Multi-rate strong tracking square-root cubature Kalman filter for MEMS-INS/GPS/polarization compass integrated navigation system. Mechanical Systems and Signal Processing, 2022, 163: 108146.
[14] ZHANG S. Research on the application of BeiDou navigation satellite system in train location of Qinghai-Tibet railway. Beijing: China Academy of Railway Sciences, 2017: 32-26.

复杂运行场景下的BDS/SINS列车组合定位方法

武晓春*, 杨伟康

兰州交通大学 自动化与电气工程学院, 甘肃 兰州 730070

摘　要： 传统的列车定位方法定位精度低，运营和维护费用高昂，无法满足列车定位技术轻量化和智能化的发展需求。针对上述问题，提出基于自适应无迹卡尔曼滤波（Adaptive unscented Kalman filter, AUKF）的北斗卫星导航系统/捷联惯导系统（BeiDou navigation satellite system/strapdown inertial navigation system, BDS/SINS）列车组合定位系统。首先，利用联合去噪算法和拉格朗日插值算法对原始数据进行预处理，消除噪声信号及异常量测值对列车定位系统的影响。其次，在标准无迹卡尔曼滤波（Unscented Kalman filter, UKF）中引入新息理论得到AUKF算法，实现系统量测噪声协方差的自适应更新。最后，在不同的铁路运行场景下，将所提AUKF与卡尔曼滤波（Kalman filter, KF）、UKF的列车定位性能进行仿真对比分析。仿真结果表明，在所有的运行场景下，AUKF计算得到的定位误差均值都小于1.5 m，定位成功率达到了95.0%。相较于KF和UKF，其定位精度和定位稳定性更好。因此，AUKF适用于运行环境复杂的铁路列车的定位服务。

关键词： 列车组合定位；北斗卫星导航系统；捷联惯性导航系统；拉格朗日插值法；联合去噪算法；自适应无迹卡尔曼滤波

引用格式： WU Xiaochun, YANG Weikang. A BDS/SINS integrated positioning approach for trains in complicated operation scenes. Journal of Measurement Science and Instrumentation, 2025, 16(3): 406-414. DOI: 10.62756/jmsi.1674-8042.2025039